# Assessment of land energy uptake in the industrial period

**Félix Garcia-Pereira**[1], **J. F. Gonzalez-Rouco**[1], **C. Melo-Aguilar**[2], **N. J. Steinert**[3], **P. De Vrese**[4], **J. H. Jungclaus**[4], **S. J. Lorenz**[4], **S. Hagemann**[5], **and E. Garcia-Bustamante**[6]

[1]**Complutense University of Madrid (UCM) and Geosciences Institute (IGEO, UCM-CSIC), Madrid, Spain** [2]IEO-CSIC, Palma de Mallorca, Spain [3]NORCE, Bergen, Norway

[4]Max Planck Institute for Meteorology, Hamburg, Germany [5]Helmholtz-Zentrum Hereon, Geesthacht, Germany [6]CIEMAT, Madrid, Spain

**Corresponding author:** Félix García-Pereira (felgar03@ucm.es)

## Abstract

Observational studies based on borehole temperature profiles provide estimates of the land component contribution to the terrestrial energy budget to be 5% in the last five decades [1,2], while the latest Coupled Model Intercomparison Project Phase 5 (CMIP5, [3]) multi-model based estimate scale it down to 2% [4]. This discrepancy stems from land surface models (LSMs) using a shallow zero-flux bottom boundary condition placement (BBCP) that severely constrains land heat uptake [4,5]. A 2100-year-long forced simulation using an improved version of the MPI Earth System Model (MPI-ESM) with a deeper BBCP (1417 m, [6,7]) captures 4 times more heat than the standard MPI-ESM CMIP6 [8] shallow BBCP (10 m) version, also well above estimates provided by other CMIP6 [9] models. However, deepening the BBCP did not affect surface temperature variability, which provides a strong basis to obtain estimates of land heat uptake from all available model and data surface temperature sources: gridded global instrumental products, reanalysis, and CMIP6 simulations. The values obtained from this new approach (9-14 ZJ in 1971-2018) are in close agreement with the values derived from the MPI-ESM1.2 deep simulation (10 ZJ), albeit still smaller than recently revised borehole-based estimates (19-25 ZJ, [1,2,10]).

## 1 Data

### The Séneca simulation

The standard CMIP6 version of MPI-ESM1.2-LR LSM, JSBACH, counts on a shallow 5-layer thermal scheme with a BBCP at 10 m. This discretization is too shallow to accommodate surface temperature variability propagation and heat uptake with depth [6,7], so it was expanded by adding 7 extra bedrock layers which deepen the BBCP to 1417 m (Fig. 1). Séneca (hereafter P2k+d) is a fully-coupled past2k simulation (0-1850) that is extended into the historical period (1850-2014) + SSP585 future scenario (2015-2100) run with the deep version of JSBACH. Its temperature variability is analyzed (Fig. 2) and compared with a past2k fully-coupled simulation run with the standard configuration of JSBACH (P2k+s). Both simulations were run using Tier 3 forcing protocol defined in Paleoclimate Model Intercomparison Project Phase 4 (PMIP4, [11]).

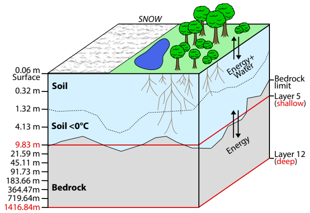


**Fig. 1. Vertical structure of the JSBACH LSM.** Red lines (numbers) indicate the downward expansion of the BBCP (depth) with seven more layers.

### Surface temperature reanalysis, observational, and model-based products

Yearly global mean temperatures at the ground surface over land (excluding glacier areas) coming from 7 global reanalyses, 5 gridded observational databases (Table S1, scan QR), and 37 first ensemble member CMIP6 [9] GCMs (Table S2) have been used in this work (Fig. 2). GST data was used for 43 of the sources (20CRv3, CERA20c, ERA20c, ERA5L, NCEP1, JRA55, and the 37 CMIP6 GCMs), while SAT was taken as a surrogate of GST evolution when this information was not available (LMRv2.1, CRUTEM5, GISTEMPv4, BEST, UDEL, and NOAAGlobalTemp).

## 2 Methodology

Global mean surrogate temperature profiles (STPs) were derived at yearly timesteps using a half-infinite one-dimensional heat conduction forward model (FM, [12,13], Eq. 1) forced by surface temperatures of the 49 data sources and P2k+ simulations. The stepwise STPs were integrated to derive land heat uptake estimates (Eq. 2). Global mean volumetric heat capacity ($C_v$) and thermal diffusivity ($\kappa$) are estimated using a bootstrap method of plausible local soil features.

**One-dimensional heat forward model**

$$STP(z) = \sum_{k=1}^{K} T(t_k)\left[erfc\left(\frac{z}{2\sqrt{\kappa t_k}}\right) - erfc\left(\frac{z}{2\sqrt{\kappa t_{k-1}}}\right)\right] \quad (1)$$

**Land heat uptake**

$$Q_s(t) = A\,\Delta z(j) \sum_{j=1}^{n} C_v(j)\,\frac{STP(t,j)+STP(t,j+1)}{2} \quad (2)$$

## 3 Results and discussion

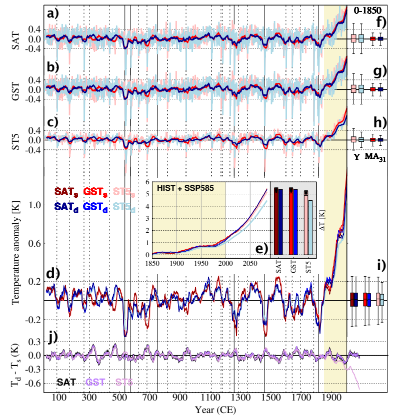


**Fig. 2. Temperature variability in Séneca.** Past2k, historical and SSP585 (P2k+) global mean SAT, GST, and ST5 anomalies (with respect 1850-1900) for both a simulation run with the MPI-ESM1.2-LR with a deep (Séneca, red) and a shallow (standard, blue) version of JSBACH.

Low-frequency variability (Fig. 2d) does not seem to be affected by deepening the LSM for surface air temperature (SAT) and ground surface temperature (GST), neither for the temperature trend during the industrial period (Fig. 2e) nor for the range of preindustrial temperature variability (Fig. 2f,g,h,i). Sudden cooling events due to volcanic activity do not show a consistent colder response for P2k+s for SAT and GST. However, there is a remarkably colder response to volcanic eruptions for P2k+s with respect P2k+d for ST5. Further, ST5 warming by the end of the 21st century for P2k+s is about 0.8 K larger than for P2k+d (Fig. 2j). Therefore, **imposing a deeper BBCP reduces temperature variability in the deepest LSM layers, yet it generates no notable response near the surface and at the ground surface.**

This entails a strong basis for using surface temperatures of different sources as boundary conditions to resolve global STPs using a FM (see section 2). These STPs are subsequently integrated to derive land uptake estimates. The methodology is proved to be capable of recovering P2k+ simulation-resolved temperature profiles (Fig. 3a) and heat uptake values (Fig. 3b).

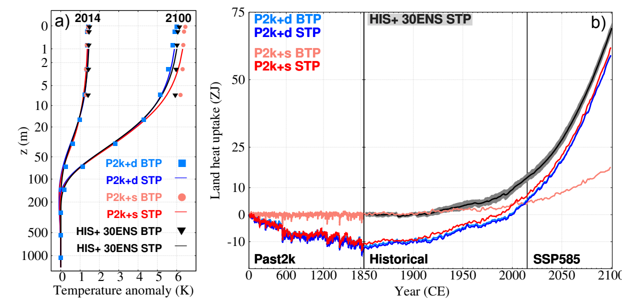


**Fig. 3. Land heat uptake in Séneca.** (a) FM STPs (continuous line) and simulated BTPs (symbols) for P2k+d (blue) and P2k+s simulations (red) and for the HIS+ 30ENS (black) in years 2014 and 2100. Y-axis is logarithmic. (b) Land heat uptake derived from the yearly time stepwise vertical integration of FM STPs and simulated BTPs for P2k+d (blue), P2k+s (red), and HIS+ 30ENS (black). The time x-axis is unevenly spaced to enhance land heat gain since 1850. For the ensemble of historical simulations, the confidence interval is also portrayed ($p < 0.05$).

Surface temperature variability of the different products used in this work is shown in Fig. 4. The 37 CMIP6 members multi-model mean yields a coordinated response of GST and SAT to forcing, with a little offset of 0.1K in 2020. That entails SAT and GST can be indistinctly used to force the FM. The reanalysis and observational gridded surface temperature anomalies lie within the range of CMIP6 multi-model variability. Nevertheless, observational sources render higher temperature anomaly values than reanalyses, showing higher temperature trends in the last decades of the historical period. All data sources indicate that land heat gain in the historical period has intensified in the last four decades (Fig. 4a), being the heat uptaken in 1971-2018 between 9 and 14 ZJ, and around 12 ZJ for CMIP6 models (Fig. 4c). This value is much higher than the 5 ZJ CMIP6 models capture when their heat uptake capability is constrained by imposing a shallow BBCP, showing the suitability of FM in correcting model-based estimates.

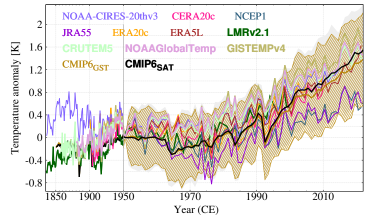


**Fig. 4.** Global mean temperature anomaly in 1850-2020 with respect to 1950 for reanalyses, observational, and a 37-member CMIP6 ensemble. SAT is plotted for observational and CMIP6 sources and LMRv2.1 (tags in bold), whereas GST is given for the remaining reanalyses and CMIP6 simulations.

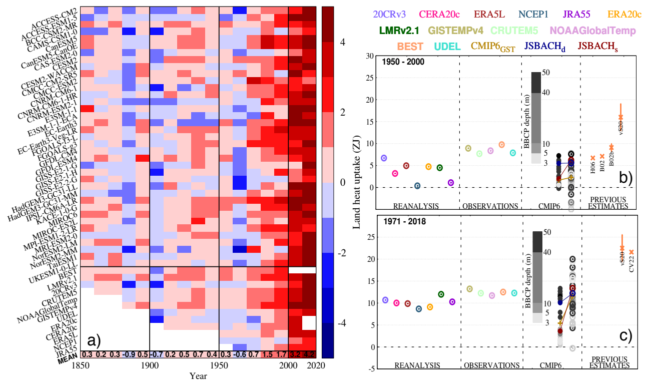


**Fig. 5.** Decadal global land heat uptake in the industrial period (1850-2020) from the different data sources in Fig. 3 (a). Land heat uptake estimates in 1960-2020 (b), and 1971-2018 (c) derived from FM STPs (hollow points) of reanalysis and observational databases, FM STPs and direct integration of CMIP6 model BTPs (solid points), and previous estimates (vS20, [1]; CV22, [2]; H06, [14]; B02, [15]; B02b, [16]; orange crosses).

Since the FM eliminates the uncertainty associated with the thermal scheme depth, **land heat uptake estimates based on this technique could be used as a proxy for climate sensitivity evaluation of model-based products**. Plausible sources of discrepancy between novel land heat estimates from different sources and previous literature [1,2,14,15,16], which are quite smaller in 1950-2000 (Fig. 4b) than in 1971-2018, are still under discussion.

## Acknowledgements

We acknowledge the financial support of the Spanish Ministry of Science to GreatModelS (RTI2018-102305-B-C21) and SMILEME (PID2021-126696OB-C21) projects, and funding FGP Ph.D.'s contract (PRE2019-090694). We would also thank the Deutsches Klimarechenzentrum (DKRZ) for the resources its Scientific Steering Committee (WLA) granted to run Séneca under project ID bm1026. We also acknowledge the effort of the World Climate Research Programme's Working Group on Coupled Modeling, responsible for CMIP, and the climate modeling groups accountable for the model simulations used herein (Table S2) in making their simulation outputs accessible.

## References

[1] von Schuckmann, K., et al. (2020). doi: 10.5194/essd-12-2013-2020.
[2] Cuesta-Valero, F. J., et al. (2022). doi: 10.5194/esd-2022-32.
[3] Taylor, K. E., et al. (2012). doi: 10.1175/BAMS-D-11-00094.1
[4] Cuesta-Valero, F. J., et al. (2016). doi: 10.1002/2016GL068496.
[5] Steinert, N. J., et al. (2021). doi: 10.1029/2021GL094273.
[6] González-Rouco, J. F., et al. (2021). doi: 10.1175/JHM-D-21-0024.1.
[7] Steinert, N. J., et al. (2021). doi: 10.1175/JHM-D-21-0023.1.
[8] Mauritsen, T., et al. (2019). doi: 10.1029/2018MS001400.
[9] Eyring, V., et al. (2016). doi: 10.5194/gmd-9-1937-2016.
[10] Forster, P., et al. (2021). doi: 10.1017/9781009157896.009.
[11] Jungclaus, J. H., et al. (2017). doi: 10.5194/gmd-10-4005-2017.
[12] Carslaw, H.S. and Jaeger, J.C. (1959). ISBN-10: 0198533683
[13] González-Rouco, J. F., et al. (2009). doi: 10.5194/cp-5-97-2009.
[14] Huang, S. (2006). doi: 10.1029/2005GL025300
[15] Beltrami, H. (2002). doi: 10.1029/2002GL015702
[16] Beltrami, H., et al. (2002). doi: 10.1029/2001GL014310

SCAN QR